Tubular Network Formation Process Using 3D Cellular Potts Model

David Svoboda(✉), Tereza Nečasová, Lenka Tesařová, and Pavel Šimara

Centre for Biomedical Image Analysis, Masaryk University, Brno, Czech Republic
svoboda@fi.muni.cz

Abstract. The simulations in biomedical imaging serve when the real image data are difficult to be annotated or if they are of limited quantity. An increasing capability of contemporary computers allows to model and simulate complex shapes and dynamic processes. In this paper, we introduce a new model that describes the formation process of a complex tubular network of endothelial cells in 3D. This model adopts the fundamentals of cellular Potts model. The generated network of endothelial cells imitates the structure and behavior that can be observed in real microscopy images. The generated data may serve as a benchmark dataset for newly designed tracking algorithms. Last but not least, the observation of both real and synthetic time-lapse sequences may help the biologists to better understand and model the dynamic processes that occur in live cells.

Keywords: 3D cellular Potts model · Virtual cell
Volumetric image data · Network formation · Fractal dimension
Lacunarity

1 Introduction

The image based simulations focused on modeling of virtual cells and their behavior started to emerge in the early 90s. Before, they represented rather a theoretical approach which was understood to be an important one but not practically used. Nowadays, namely due to the increasing computational power, availability of multi-core processors or GPUs, and the capacity of contemporary computers, the development of new cell simulation frameworks goes hand in hand with newly emerging algorithms handling the biomedical image data. The current simulation frameworks can generate the synthetic image data accompanied with absolute ground truth in large quantities. The simulated data are either static [2,5] or dynamic [1,12].

The static data typically correspond to some images acquired with confocal or widefield fluorescence microscope. With this acquisition technique, only the subcellular components, that are under the scope, are fluorescently labeled and therefore visualized. This fact markedly simplifies the generated model of cell as there is no need to understand the whole cellular structure. On the other hand,

A. Gooya et al. (Eds.): SASHIMI 2018, LNCS 11037, pp. 90–99, 2018.
https://doi.org/10.1007/978-3-030-00536-8_10

the staining procedure, that precedes the acquisition of real images, takes some time. Moreover, in live cell imaging the staining may influence the behavior of the observed cells. For this purpose a phase contrast microscopy serves as an alternative solution and is very popular. This advantage is counterbalanced by the fact, that the synthetic model has to describe the whole cell structure and must be defined fully in 3D. The model, that would combine both or even multiple modalities (bright field microscopy [6], TIRF [8], or SMLM [9]) together, is a holy grail of simulations.

Even though there have been designed and implemented many simulation frameworks suitable for generation of time-lapse image sequence [15], most of them provided rather a schematic and simplified data. In [1], for example, the objects under the scope were the cells represented simply by touching or overlapping spheres without any internal structure. In [12], the authors proposed a generator of a cell population. The cells were allowed to move and split due to mitosis. Nevertheless, the interaction between the cells was rather limited. In agent-based approach, the biologically motivated model is based on the modification [7] of standard cellular Potts model (CPM) [4] where the cells are expected to markedly interact. This approach was further extended [13] and the cells were allowed to be elongated as chords to resemble the behavior of real endothelial cells in tubular networks (see Fig. 1). The model was, however, settled in 2D only. This fact on one hand brings the advantage of high speed computation. On the other hand, the manipulation with 2D image data is very limiting, namely when simulating the behavior of phase contrast microscope, where the full 3D image information is required. In 2012, Scianna and Preziosi [10] designed a straightforward extension of Merks' model into 3D. Later on, Svoboda and Kozubek [14] simplified Sianna's model and added the final post processing simulating the fluorescence as well as phase contrast microscope. Nevertheless, none of these two approaches offered a generation of straight elongated cells that occur in real images of tubular networks due to tension of the whole network. The tension forces caused some cells to be either unnaturally deformed or disjoint. In some particular cases some cells were even torn into pieces.

In this paper, we introduce a modification of previously mentioned CPM-based models. The newly presented model is defined fully in 3D space, keeps the already established mutual cell connections and guarantees the presence of chord-like cells that are exposed to tension forces. The synthetic image data produced by our approach are presented. A validation of similarity of both real and synthetic data using the fractal dimension and lacunarity descriptors is also provided.

2 Method

The proposed model combines the basic principles introduced in [10,14]. Let us first recall these principles. Afterwards, we emphasize the differences and introduce the new approach.

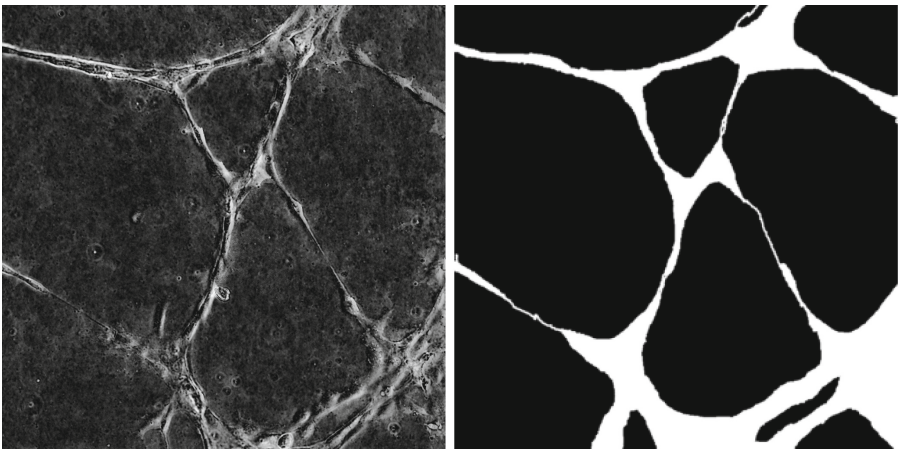

Fig. 1. An example of cell population forming a tubular network: (left) real image acquired using a phase-contrast microscope; (right) the left image annotated using two classes – foreground and background. Note, that all the images are volumetric ones. In order to visualize them we used maximum intensity projection.

2.1 3D Cellular Potts Model

Basic Definitions. Let $\Omega \subset \mathbb{R}^3$ be a three-dimensional lattice with each grid site $\mathbf{x} \in \Omega$ labeled with a spin function $\sigma \subset \Omega \times (\texttt{LABELS} \times \mathbb{N}_0 \times \mathbb{N}_0)$

$$\sigma : \mathbf{x} \rightarrow (label, id, cell). \tag{1}$$

where the individual elements have the meaning as follows:

- The property *label* defines the type of biological structure that the currently inspected grid site belongs to. The following set $\texttt{LABELS} = \{\texttt{nucleus}, \texttt{cytoplasm}, \texttt{mitochondrion}, \texttt{medium}, \texttt{ECM}\}$ is used. The first three labels correspond to subcellular components. The last two labels define the non-cellular objects appearing in the biological specimens. They are usually understood as a background. Here, `ECM` stands for *extra cellular matrix*.
- Inside each cell, there is just one nucleus. Nevertheless, some components appear twice or even multiple times. In order to distinguish between the individual occurrences of such objects a unique identifier $id \in \mathbb{N}_0$ is introduced. All the components are surrounded by the cytoplasm which is associated with one unique *id*.
- An element $cell \in \mathbb{N}_0$ is a unique identifier of a cell to which the currently inspected grid site $\mathbf{x}$ belongs.

In order to simplify the notation, let us define the name substitution $\sigma_{\text{bg}} = (bgLabel, 0, -)$, where $bgLabel \in \{\texttt{medium}, \texttt{ECM}\}$. The term σ_{bg} is therefore a value of spin function σ in a lattice site $\mathbf{x}$ that belongs to `medium` or `ECM`.

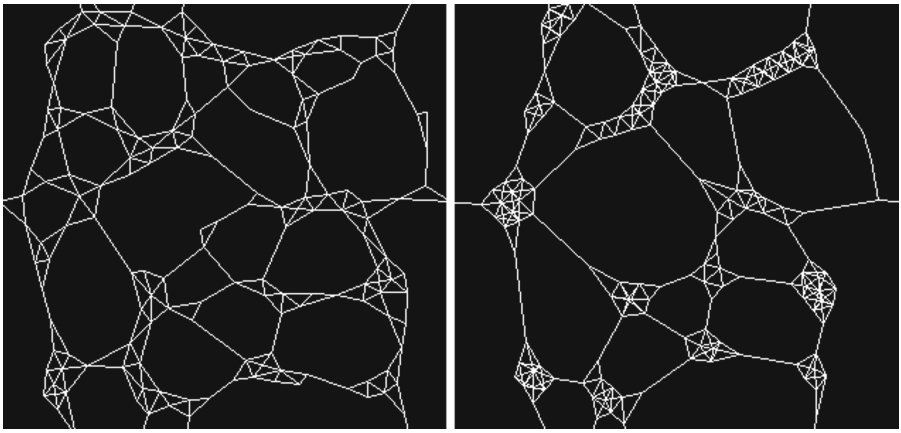

Fig. 2. An example of connectivity graph G: (left) shape of graph during the network evolution, (right) final configuration of the graph. Please note, that both graphs are defined fully in 3D. For visualization purposes a maximum intensity projection was used.

Finally, let $\pi_i, i \in \{1, 2, 3\}$ be a projection function that takes an element $\mathbf{x} = (x_1, x_2, x_3)$ of the Cartesian product $(X_1 \times X_2 \times X_3)$ to the value $\pi_i(\mathbf{x}) = x_i$. By using this projection, we can get, for example, the label of one particular grid site $\mathbf{x}$ by evaluating the term $\pi_1(\sigma(\mathbf{x}))$.

The 3D lattice Ω with its sites and spin function σ can be also understood as a discrete multichannel 3D image with individual voxels and voxel values. The voxels with similar values form the logical objects that we want to represent using the lattice Ω. In this case, the objects are the cells and their components.

Connectivity Preservation. In order to control the connectivity of neighboring cells, the graph based approach that tackles with the connectivity of CPM [13,14] is utilized. Here, a geometrical center of each cell is understood to be a vertex. The edge between two vertices is established if the corresponding cells touch using at least one voxel. This way, a non-oriented graph $G = (V, E)$ is constructed. Let $v \in V$ be any vertex in the graph G, then $d_G(v)$ is a number of all edges originating from v. In the very beginning, the graph G is disconnected, i.e., $\forall v \in V : d_G(v) = 0$. During the time, the nearby cells tend to join and the graph structure changes (see Fig. 2).

System Dynamics. The evolution of CPM is an iterative process that starts with an random initial distribution of cells rendered in the lattice Ω. One iteration of the CPM suggests to flip the spin function of a randomly selected grid site $\mathbf{x}_s$ (source) to a spin function $\sigma(\mathbf{x}_t)$ of its randomly selected neighbor $\mathbf{x}_t$ (target), and evaluates how this flip would affect the Hamiltonian H of the whole system:

$$\Delta H = \Delta H_{Adhesion} + \Delta H_{Shape} + \Delta H_{Chemotaxis}. \tag{2}$$

The term $H_{Adhesion}$ expresses the desire of individual grid site to either stay in contact with each other or to stay alone.

$$H_{Adhesion} = \sum_{\mathbf{x}\in\Omega,\mathbf{x}'\in N_x} \left(1 - \delta_{\sigma(\mathbf{x}),\sigma(\mathbf{x}')}\right) J(\pi_1(\sigma(\mathbf{x})), \pi_1(\sigma(\mathbf{x}'))) \tag{3}$$

Here, $\delta_{x,y}$ is the Kronecker delta, $N_{\mathbf{x}}$ is a set of sites neighboring to $\mathbf{x}$. Finally, the $J \subset (\texttt{LABELS} \times \texttt{LABELS}) \times \mathbb{N}$ is a function that associates the binding penalties for individual pairs of components and is defined by an enumeration:

$J(\texttt{cytoplasm}, \texttt{ECM}) = 30$
$J(\texttt{cytoplasm}, \texttt{medium}) = 40$
$J(\texttt{cytoplasm}, \texttt{cytoplasm}) = 10$
$J(\texttt{cytoplasm}, \texttt{nucleus}) = 40$
$J(\texttt{cytoplasm}, \texttt{mitochondrion}) = 40$
$J(\texttt{medium}, \texttt{ECM}) = 0$
$J(\texttt{ECM}, \texttt{ECM}) = 0$
$J(\texttt{medium}, \texttt{medium}) = 0$
$J(other, other) = 10000$

The term H_{Shape} imposes geometrical constrains. In this case, the cell volume (number of grid sites per cell) constraint is employed:

$$H_{Shape} = \lambda_{volume} \sum_{L,C} \left(vol_{L,C} - Vol_L\right)^2 \tag{4}$$

where λ_{volume} is a weight defining the influence of this term, C is an cell id, L is a cell component id, $vol_{L,C}$ is the current volume of a component L in cell C, and Vol_L is an mean expected volume of components with label L.

The term $\Delta H_{Adhesion}$ (ΔH_{Shape}) expresses the difference between $H_{Adhesion}$ (H_{Shape}) calculated with the new suggested value of $\sigma(\mathbf{x}_t)$ and $H_{Adhesion}$ (H_{Shape}) with the original value $\sigma(x_s)$.

Finally, the term $\Delta H_{Chemotaxis}$ expresses the cell ability to respond to the chemical stimulus. Each cell detects the concentration of signals (the biological material which is produced by each cell and which serves as an attractor to other cells) in its vicinity and tries to occupy the position with the highest positive gradient of concentration $c(\cdot,\cdot)$. The term is expressed as:

$$\Delta H_{Chemotaxis} = -\left(1 - \delta_{\sigma(\mathbf{x}_s),\sigma_{\mathrm{bg}}}\right) \lambda_{chemical} \left[c(\mathbf{x}_t, t) - c(\mathbf{x}_s, t)\right] \tag{5}$$

where $\lambda_{chemical}$ is a parameter controlling the importance of cell chemotaxis and $c(\mathbf{x}, t)$ is the current (time t) concentration of the signals at the site $\mathbf{x}$. The term $c(\mathbf{x}_t, t) - c(\mathbf{x}_s, t)$ defines the difference in concentrations between the current $\mathbf{x}_s$ and the proposed $\mathbf{x}_t$ sites. The concentration function $c(\cdot,\cdot)$ is defined by the following equation (arguments were dropped):

$$\frac{\partial c}{\partial t} = D\nabla^2 c + \beta(\mathbf{x}, t)(1 - \delta_{\sigma(\mathbf{x}),\sigma_{\mathrm{bg}}}) - \frac{1}{\gamma}\delta_{\sigma(\mathbf{x}),\sigma_{\mathrm{bg}}}\, c \tag{6}$$

where $\beta(\mathbf{x}, t)$ is the secretion rate of the signals released from the cell that occupies the site $\mathbf{x}$, γ is the half life of signals in the medium, and D is the diffusion coefficient. The secretion rate β is a decreasing function, i.e., if given

cell acquires sufficient number of attachments with surrounding cells, it decreases the production of signals c:

$$\beta(\mathbf{x}, t) = \begin{cases} \alpha \cdot 0.9995^{(t-t_0)} & \text{if} \quad d_G(\pi_3(\sigma(\mathbf{x}))) \geq 2 \\ \alpha & \text{otherwise} \end{cases} \tag{7}$$

Here, α is a initial secretion rate identical for all the cells, and t_0 is the time when the given cell $\pi_3(\sigma(\mathbf{x}))$ first attached at least two other cells.

The probability of flipping the spin of the lattice site $\mathbf{x}_s$ to the spin $\sigma(\mathbf{x}_t)$ is then given as:

$$P\left(\sigma(\mathbf{x}_t) \leftarrow \sigma(\mathbf{x}_s)\right) = \begin{cases} e^{-\Delta H/T} & \text{if } \Delta H > 0, \\ 1 & \text{if } \Delta H \leq 0. \end{cases} \tag{8}$$

where T is a temperature describing the willingness of cells to move.

2.2 The Proposed Modifications

Intra-Cell Compactness. In [7], Merks et *al.* introduced a method that kept each cell to be compact. The algorithm took the pixel, which value was proposed to be changed, and compared it with the values of its neighbors. The check for the local compactness was based on the inspection of individual neighbors in the clock-wise manner. Unfortunately, this approach could not be straightforwardly extended to 3D space. For this purpose, we propose a new method which works well for 3D and can be extended to any higher dimension. The procedure checks if the proposed change of the value in the inspected voxel would keep or violate the compactness of the cell to which this voxel belongs. The procedure is as follows:

1. Let $\mathbf{x} \in \Omega$ be an inspected voxel belonging to some cell and let $N_{\mathbf{x}}$ be its $3 \times 3 \times 3$ neighborhood.
2. Collect the labels from grid Ω in the neighbourhood $N_{\mathbf{x}}$, keep their positions, and create a 3D labeled image K as follows: $\forall \mathbf{p} \in N_{\mathbf{x}} : K(\mathbf{p} - \mathbf{x}) = \pi_1(\sigma(\mathbf{p}))$.
3. Count, how many voxels in K belong to background (`medium` or `ECM`) and store the result as value a.
4. Count, how many different labels are included in K and store the result as value b.
5. Derive a binary image K_b from K by setting voxels with the same label, as the central voxel has, to *true*.
6. Set the central voxel value in K_b to *false* to simulate the proposed voxel value change.
7. Find any voxel with value *true* in K_b and run the flood-fill algorithm starting from this voxel. The filling value is *false*.
8. Try to find again any voxel with value *true* in K_b.
9. If the last search was successful and ($a > 0$ or $b \geq 2$)) then mark the proposed voxel value change in $\mathbf{x}$ as undesirable as this change would split the cell into at least two pieces.

Tension Forces. The tension and stress inside the network is strongly influenced by the chemotactic term (5). In the following text, we propose a modification of this term and, afterwards, check how it influences the formation of network structure in 3D space.

As soon as some cell detects a remarkable drop of signal concentration c in its vicinity, it starts to starve. We propose this cell to stop using the term $\Delta H_{Chemotaxis}$ and also all the cells reachable from this cell through the graph G change their behavior analogously.

Due to the proposed change, the term $\Delta H_{Adhesion}$ becomes more dominant. Together with the shape term ΔH_{Shape} it keeps the volume of each cell at a given mean value and pushes each cell to have the lowest possible surface. This constraint applied to two neighboring connected cells, that are pulled from each other, produces elongated and smoothly thinning connection. This is, however, not the case of 3D model, where the lowest possible surface requires the cells to look like ideal spheres, while connections are formed of unnaturally twisted one voxel wide curves. The difference stems from the fact, that 2D model is a just a cross section of the 3D model and does not properly describe the real organization of cells in 3D space. In order to get smoothly thinning and strain connection between each two connected cells in 3D model, we propose the following modification of each CPM iteration:

1. Take a current graph G and render it into the image of the same size as the lattice Ω is (see an example in Fig. 2).
2. Compute the 3D Euclidean distance map (EDM) over this image.
3. If a grid site $\mathbf{x}$, that belongs to some cell, is proposed to become a background grid site (`medium` or `ECM`) and the EDM($\mathbf{x}$) $< width$, where $width$ is a minimum acceptable width of the connection between the cells, we reject this change proposal.

3 Results and Validation

The objective of this paper was to propose a model that describes the structure of the tubular network and its evolution in the course of time. From the biological point of view, the most important aspect is the final configuration of the network. The biologists inspect the structure of the network and the organization of the cells. For this reason, we focus our interest on the generated images that record the network in a stable configuration, i.e., when it stops evolving. In Fig. 3, you can see a sample final network as a rendered volumetric image. As it is difficult to imagine the exact shape of the network in the perspective projection, we also offer a maximum intensity projection of this particular network in Fig. 4 (bottom-left image). In the given figure, you can also inspect other synthetically generated networks (bottom row) and visually compare them with the real networks (upper row), that were obtained by manual annotation of real microscopy images.

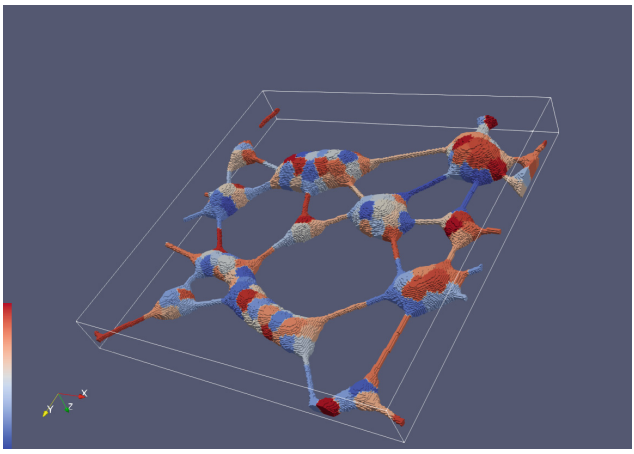

parameter	value
$width$	2
$\lambda_{chemical}$	6000
T	50
λ_{volume}	50
α	0.0025
D	1×10^{-13}
$\lvert N_x \rvert$	26
γ	800

Fig. 3. 3D visualization of synthetic tubular network using Paraview software together with a list of parameters that were used for the creation of this artificial network.

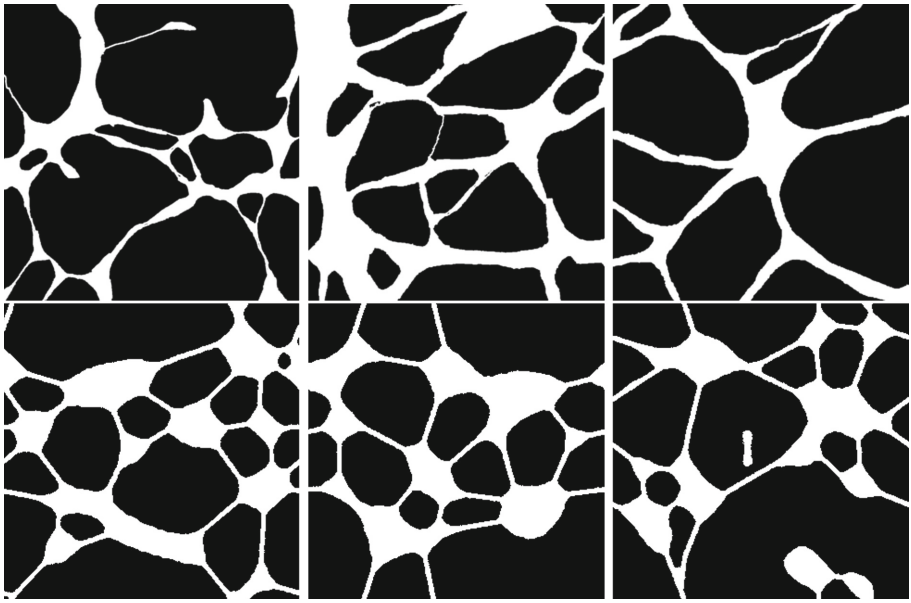

Fig. 4. A collection of images representing the mask of tubular network of endothelial cells. The first row contains the real images, the second one the synthetic ones. For the visualization purposes, the maximum intensity projection is utilized.

In order to validate our model, we decided to employ the standard measures that describe the complexity of the structures depicted in the analyzed images: *box counting fractal dimension* and *lacunarity* [3,11]. As a tool for computation of these two measures we employed the *ImageJ* software[1] together with the *FracLac* plugin[2]. Both ImageJ and FracLac are freely available.

Seven representatives from real data were randomly selected for annotation and used for comparison to seven randomly selected representatives from synthetic data. The analysis of these images was performed using a linear mixed model. The main objective was to inspect the effect of being a synthetic or real image on the value of fractal dimension or lacunarity with respect to the random effects given by 12 different measurements for each of 14 individual images (7 synthetic + 7 real). The estimated effect of synthetic data on fractal dimension was $\beta = 0.031$ (standard error: 0.018), which was not significant (p-value = 0.137, level of significance $\alpha = 0.05$). In case of lacunarity the change was $\beta = -0.068$ (standard error: 0.096) for synthetic data compared to real data, which was not significant (p-value = 0.666, level of significance $\alpha = 0.05$). Thus, there were no significant differences between the real and synthetic data in terms of fractal dimension and lacunarity. (The logarithm transformation was used for the values of fractal dimension prior to the model construction.)

4 Conclusions

In this paper, we proposed a modification of 3D CPM model that is able to describe the structure and evolution of the tubular network of living endothelial cells. In order to check the plausibility of computer generated data, we submitted both real and synthetic images to selected image descriptors and showed a high level of similarity between both categories.

The proposed model (the implementation is freely available[3]) and the generated data can be used for the verification of some biological hypothesis and subsequently to better understanding of dynamic processes that occur in live cells. In the future, we also plan to properly simulate the optics of phase contrast microscope to be able to create real-like looking images resembling the images acquired from the real microscope. In this sense, we would be able to produce image datasets suitable for the tasks including image segmentation, tracking or reconstruction.

Acknowledgments. This work was supported by Czech Science Foundation, grant No. GA17-05048S.

[1] https://imagej.net/.
[2] https://imagej.nih.gov/ij/plugins/fraclac/fraclac.html.
[3] https://cbia.fi.muni.cz/research/simulations/multicomponent-cpm.html.

References

1. Dufour, A., Thibeaux, R., Labruyère, E., Guillén, N., Olivo-Marin, J.C.: 3-D active meshes: fast discrete deformable models for cell tracking in 3-D time-lapse microscopy. IEEE Trans. Image Process. **20**(7), 1925–1937 (2011)
2. Ghaye, J., Micheli, G., Carrara, S.: Simulated biological cells for receptor counting in fluorescence imaging. BioNanoScience **2**, 94–103 (2012)
3. Gould, D.J., Vadakkan, T.J., Poché, R.A., Dickinson, M.E.: Multifractal and lacunarity analysis of microvascular morphology and remodeling. Microcirculation **18**, 136–151 (2011)
4. Graner, F., Glazier, J.A.: Simulation of biological cell sorting using a two-dimensional extended Potts model. Phys. Rev. Lett. **69**(13), 2013–2016 (1992)
5. Lehmussola, A., Ruusuvuori, P., Selinummi, J., Huttunen, H., Yli-Harja, O.: Computational framework for simulating fluorescence microscope images with cell populations. IEEE TMI **26**(7), 1010–1016 (2007)
6. Malm, P., Brun, A., Bengtsson, E.: Papsynth: simulated bright-field images of cervical smears. In: International Symposium on Biomedical Imaging: From Nano to Macro, pp. 117–120. IEEE Press (2010)
7. Merks, R.M., Brodsky, S.V., Goligorksy, M.S., Newman, S.A., Glazier, J.A.: Cell elongation is key to in silico replication of in vitro vasculogenesis and subsequent remodeling. Dev. Biol. **289**(1), 44–54 (2006)
8. Rezatofighi, S.H., et al.: A framework for generating realistic synthetic sequences of total internal reflection fluorescence microscopy images. In: International Symposium on Biomedical Imaging, pp. 157–160 (2013)
9. Sage, D., et al.: Quantitative evaluation of software packages for single-molecule localization microscopy. Nat. Methods-Tech. Life Sci. Chem. **12**(8), 717–724 (2015)
10. Scianna, M., Preziosi, L.: Multiscale developments of the cellular Potts model. Multiscale Model. Simul. **10**(2), 342 (2012)
11. Smith, T., Lange, G., Marks, W.: Fractal methods and results in cellular morphology - dimensions, lacunarity and multifractals. J. Neurosci. Methods **69**(2), 123–136 (1996)
12. Svoboda, D., Ulman, V.: MitoGen: a framework for generating 3D synthetic time-lapse sequences of cell populations in fluorescence microscopy. IEEE Trans. Med. Imaging **36**(1), 310–321 (2017)
13. Svoboda, D., et al.: Vascular network formation in silico using the extended cellular Potts model. In: IEEE International Conference on Image Processing, pp. 3180–3183, September 2016
14. Svoboda, D., Kozubek, M.: Multimodal simulations in live cell imaging. In: Tsaftaris, S.A., Gooya, A., Frangi, A.F., Prince, J.L. (eds.) SASHIMI 2017. LNCS, vol. 10557, pp. 89–98. Springer, Cham (2017). https://doi.org/10.1007/978-3-319-68127-6_10
15. Ulman, V., Svoboda, D., Nykter, M., Kozubek, M., Ruusuvuori, P.: Virtual cell imaging: a review on simulation methods employed in image cytometry. Cytom. Part A **89**(12), 1057–1072 (2016)